

Viking Orbiters 1 and 2 Radio Occultation Electron Density: User Guide

Paul Withers (withers@bu.edu) (Boston University)

Version 1.0

01 Jan 2020

Contents

1	Scope	6
2	Introduction	6
3	Ionospheric observations by Viking Orbiters 1 and 2 radio occultations	8
4	Availability of data from Viking Orbiters 1 and 2 radio occultations	10
5	Validation of electron density profiles supplied by Breus	11
5.1	Information supplied by Breus	11
5.2	Validation against published images of profiles	12
5.3	Instances of duplicate profiles	13
5.4	Summary of validation activities	16
6	Provenance of electron density profiles supplied by Breus	16
7	Uncertainties in electron density values	17
8	Ancillary information	18
9	Definition of altitude	20
10	Completeness of set of profiles supplied by Breus	22
11	Overview of electron density measurements	24
12	Archive organization and naming	25
12.1	Logical identifiers	25
12.1.1	LID formation	25
12.1.2	VID formation	26
12.2	Archive contents for the <code>voroelden</code> bundle	26
12.2.1	<code>voroelden:data_derived</code> data collection	27

12.2.2	Description of electron density data products	27
12.2.3	<code>voroelden:document</code> document collection	28
13	Archive product formats	28
13.1	Data file formats	28
13.2	PDS labels	30
14	Summary	30
15	Acknowledgements	31
16	References	32
17	Tables	35
18	Figures	41

List of Tables

1	Summary of Viking Orbiters 1 and 2 electron density profiles.	36
---	---	----

List of Figures

1	(left) Profile from Viking Orbiter 1 on orbit 181. (right) Profiles from Viking Orbiter 1 on orbits 610 (left), 612, 617, 622, 625, 626, and 639 (right). Densities in the i -th profile are multiplied by a factor of $10^{(i-1)}$ in order to offset profiles for clarity. That is, densities in the first profile (orbit 610) are multiplied by a factor of $10^0 = 1$ and densities in the seventh profile (orbit 639) are multiplied by a factor of 10^6 . Reproduction of Figure 9b of <i>Zhang et al.</i> (1990a).	42
2	(left) Peak electron density as a function of solar zenith angle (crosses). The solid line is a fit from <i>Hantsch and Bauer</i> (1990). Reproduction of Figure 1 of <i>Hantsch and Bauer</i> (1990). (right) Peak altitude as a function of solar zenith angle (crosses). The solid line is a fit from <i>Hantsch and Bauer</i> (1990). Reproduction of Figure 3 of <i>Hantsch and Bauer</i> (1990).	43
3	(left) Profiles from Viking Orbiter 1 on orbits 289 (black), 523 (grey), and 755 (red). The vertical blue line indicates zero. (right) Profiles from Viking Orbiter 1 on orbits 490 (black), 508 (grey), and 523 (red). The vertical blue line indicates zero.	44
4	(left) Primary (black) and secondary (grey) representations of the profile from Viking Orbiter 1 on orbit 769. (right) Primary (black) and secondary (grey) representations of the profile from Viking Orbiter 2 on orbit 149.	45
5	(top left) Dependence of N_{min} on solar zenith angle. (top right) Dependence of N_{top} on solar zenith angle. (bottom left) Dependence of $SDEV5$ on solar zenith angle. (bottom right) Dependence of $RMS5$ on solar zenith angle.	46
6	Profiles from Viking Orbiter 1 egress occultations on orbits 225 (black), 227 (grey), and 229 (red). The vertical blue line indicates zero.	47

7	(left) Time series of solar zenith angles sampled by electron density profiles from Viking Orbiters 1 and 2 radio occultations. Black symbols indicate Viking Orbiter 1 profiles, grey symbols indicate Viking Orbiter 2 profiles. (right) Geographic coverage of electron density profiles from Viking Orbiters 1 and 2 radio occultations. Colors indicate solar zenith angle.	48
8	(left) Five selected profiles from Viking Orbiter 1 at solar zenith angles near 50° (orbit 490, black), 60° (orbit 766, grey), 70° (orbit 609, cyan), 80° (orbit 594, green), and 90° (orbit 292, red). The blue vertical line highlights zero. (right) As left panel, but with a logarithmic axis.	49
9	(left) Dependence of electron density on solar zenith angle and altitude. Regions without data are shown in white. The number of profiles in each solar zenith angle bin is noted at high altitude. (right) Electron density measurements from the left panel at altitudes of 120–125 km (black), 160–165 km (grey), 200–205 km (red), and 240–245 km (blue).	50

1 Scope

This user guide describes derived data products from Viking Orbiters 1 and 2 radio occultations at Mars and their accompanying documentation. The derived data products are Mars ionospheric electron density profiles from radio occultations.

Note that this document is effectively divided into three parts. Sections 2–11 describe the generation and validation of the derived data products. Sections 12–13 are PDS-specific. They describe archive organization, data product formats, and naming conventions. Sections 14–18 contain summary, acknowledgements, references, tables, and figures.

The structure of this document is as follows. Section 2 introduces the document. Section 3 describes the ionospheric observations by Viking Orbiters 1 and 2 radio occultations. Section 4 discusses the availability of data from Viking Orbiters 1 and 2 radio occultations. Section 5 describes how electron density profiles were validated. Section 6 describes the provenance of the archived data set. Section 7 describes how uncertainties were assigned to electron density values. Section 8 describes how essential ancillary information for each observation was obtained. Section 9 describes the altitude convention used for the vertical coordinate of the archived electron density profiles. Section 10 discusses the completeness of the set of electron density profiles. Section 11 presents an overview of the archived electron density profiles. Section 12 describes the archive organization. Section 13 describes the format of archived data products. Section 14 presents a summary of this document. Section 15 offers acknowledgements. Section 16 lists references. Section 17 contains tables. Section 18 contains figures.

2 Introduction

The Viking Orbiters were an integral part of the most significant planetary exploration mission of the 1970s (*Soffen, 1977; Kieffer et al., 1992*). Their cameras showed that Mars has a rich, dynamic, and apparently wet geological history, their infrared thermal mappers (IRTMs) performed the first systematic monitoring of the atmospheric climate, and their water vapor

mapping (MAWD) revealed the water cycle that couples the surface, atmosphere, and poles. The Viking Orbiters also conducted radio occultation observations (*Fjeldbo et al.*, 1977; *Lindal et al.*, 1979). An occultation occurs when the line-of-sight between the spacecraft and Earth is obstructed by the solid body of Mars. Just before and after the occultation, the radio signal passes through the atmosphere and is modified by it. When the spacecraft's orbital plane is nearly edge-on as seen from Earth, two occultations occur per orbit, one when the spacecraft goes behind Mars (ingress) and one when the spacecraft comes out from behind Mars (egress). When the spacecraft's orbital plane is near face-on as seen from Earth, occultations do not occur.

For an ionospheric occultation observation, an antenna of the Deep Space Network (DSN) transmitted a carrier-only uplink signal at S-band to the spacecraft. The spacecraft received this signal, then coherently retransmitted it at two frequencies, S-band and X-band. "The exact ratio between the S and X band downlink carrier frequencies transmitted from the spacecraft is 3/11" (*Fjeldbo et al.*, 1977). These two downlink signals were received on the ground at the same antenna (often one of the DSN's three 64-m antennas). Due to the limited performance of the onboard oscillator, ionospheric observations required two-way coherent lock such that all frequencies were referenced to the stable oscillator at the ground station.

Radio occultations by Viking Orbiters 1 and 2 produced three main data products: a pre-MOLA topographic map (based on where radio signals were obscured by the solid body of the planet), vertical profiles of neutral atmospheric density, pressure, and temperature, and vertical profiles of ionospheric electron density (*Fjeldbo et al.*, 1977; *Lindal et al.*, 1979). Although the broad suite of radio science investigations on the Viking Landers and Orbiters was led by W. H. Michael (*Snyder and Moroz*, 1992), the radio occultations were led by Fjeldbo (who changed his name to Lindal in 1978).

"The first step in the analysis of the radio frequency data consists of computing the Doppler perturbations imposed on the links by the Martian atmosphere. The differential dispersive downlink Doppler, defined as the received S band frequency minus 3/11 of the X

band frequency, is used to study ionization in the atmosphere of Mars. The effects of plasma changes in the solar corona and the terrestrial ionosphere are approximated by subtracting a linear frequency term from the data. This frequency drift term is determined by fitting a straight line in a least squares sense to the differential dispersive Doppler data obtained above the Martian atmosphere” (*Fjeldbo et al.*, 1977). Ionospheric electron density profiles were derived from the differential dispersive Doppler data by *Fjeldbo et al.* (1977) and *Lindal et al.* (1979) using standard methods (e.g., *Dalba and Withers*, 2019). These measurements of electron densities in the ionosphere of Mars are the focus of this document.

3 Ionospheric observations by Viking Orbiters 1 and 2 radio occultations

Viking Orbiters 1 and 2 conducted radio occultations at Mars from 1976 to 1978 (*Lindal et al.*, 1979; *Kliore*, 1992). Viking Orbiter 2 ceased operations in July 1978. Although Viking Orbiter 1 continued operations until August 1980, no further radio occultation measurements were collected.

Surprisingly, the Viking Orbiter electron density profiles were not studied intensively at the time of this mission, possibly because ionospheric scientists were focused on the unprecedented Viking Lander data on the chemical composition of the thermosphere, chemical composition of the ionosphere, and energetics of the ionosphere (e.g., *Chen et al.*, 1978), rather than on the opportunities made possible by the addition of ~ 100 Viking electron density profiles to the existing set of ~ 100 Mariner 9 electron density profiles (*Withers et al.*, 2015).

Interest in the Viking Orbiter electron density profiles was stimulated by developments at Venus, where the Pioneer Venus Orbiter mission acquired extensive measurements of the planet’s upper atmosphere, ionosphere, and plasma environment during the 1980s (*Mutch*, 1980; *Hunten et al.*, 1983). As that mission approached its end, scientists realized that many of the discoveries made at Venus might also be applicable at Mars and an active period of

comparative studies of the ionospheres of Venus and Mars began. Viking electron density profiles were used for such studies by *Zhang et al.* (1990a,b); *Woo and Kliore* (1991); *Kliore* (1992); and *Breus et al.* (1998a,b). They were also re-interpreted by *Ness et al.* (2000) in light of the MGS discovery of crustal magnetic field regions on Mars. One further publication used the Viking electron density profiles to characterize the effects of solar zenith angle and solar irradiance on ionospheric peak densities and peak altitudes, though without discussing the source of the data (*Hantsch and Bauer*, 1990).

The Viking Orbiter radio occultation electron density profiles represent unique and valuable observations of the ionosphere of Mars that have not been superseded by the widely-used set of 5600 MGS radio occultation ionospheric profiles. Relative to the MGS dataset, the Viking Orbiter dataset has some unique characteristics:

1. Better sensitivity. The smallest electron density reported in each Viking Orbiter profile is approximately equal to the electron density uncertainty for that profile. The average of these smallest densities, $1.4 \times 10^9 \text{ m}^{-3}$, is more than three times smaller than the average uncertainty in the MGS electron densities, $4.6 \times 10^9 \text{ m}^{-3}$ (*Withers*, 2010). The dual frequency experiment of Viking eliminated some uncertainties that affected the single frequency measurements of MGS. Also, the 400 km circular orbit of MGS meant that the pre-occultation baseline, an important part of the data processing, was always affected by plasma in the 200–400 km range.

2. Higher vertical extent. Half of the Viking Orbiter profiles extend higher than 250 km, whereas MGS profiles rarely exceed 200 km. This is due to Viking’s better sensitivity.

3. Global coverage. The Viking Orbiter profiles are globally distributed, whereas almost all of the 5600 MGS profiles are north of 60°N. The only ones that are not are 220 profiles between 70°S and 64°S. The Viking Orbiter profiles permit exploration of the ionosphere within the tropical neutral atmosphere and above a range of crustal magnetization conditions.

4. Solar zenith angle coverage. Solar zenith angle, or how high the Sun is in the sky, is the major factor controlling ionospheric conditions on Mars. All MGS profiles have solar zenith angles of 71 degrees or more, where the Sun is very low on the horizon. By contrast,

the Viking Orbiter profiles sample solar zenith angles as low as 50 degrees, closer to the subsolar point.

4 Availability of data from Viking Orbiters 1 and 2 radio occultations

Unfortunately, the high-level data products of the Viking radio occultation investigation, the atmospheric and ionospheric profiles, were not archived. These electron density profiles are not currently available to the scientific community in a digital format. As part of a wide-ranging program to acquire and archive ionospheric electron density profiles from radio occultation experiments, we conducted a search for the Viking electron density profiles.

At the Planetary Data System, Viking data products are curated by the Geosciences Node (<https://pds-geosciences.wustl.edu/missions/viking/index.htm>). All available radio science products concern gravity tracking, but none concern occultation observations. The NASA Space Science Data Coordinated Archive (NSSDC) also curates Viking data products. The NSSDC lists approximately 15 data collections associated with orbital radio science.

Data collection PSPG-00406 (previously labeled 75-075A-04B) provides date, time, and S-band and X-band received frequencies for occultation observations from 6 October 1976 to 1 November 1976. It is available in digital form to potential users. We have acquired and inspected a copy of this data collection. In principle, ionospheric electron density profiles can be obtained from this information. Yet these data were acquired near solar conjunction at Sun-Earth-Mars angles of 7° – 14° and were severely degraded by radio phase scintillations in the solar corona (*Fjeldbo et al.*, 1977). “It was nevertheless possible to detect layers similar to those reported earlier [by Mariner 9]” (*Fjeldbo et al.*, 1977). However, no ionospheric profiles from this period are discussed or acknowledged in any subsequent publications, suggesting that the data quality was eventually deemed unacceptable. Therefore we have not attempted to derive ionospheric electron density profiles from the NSSDC PSPG-00406 data collection.

Data collection PSPG-00147 (previously labeled 75-083A-04E) is stated to contain “radio

occultation observations”. It is stated to contain relevant time and frequency information, but the date range covered is not stated in the available description of the data collection. The NSSDC characterizes this data collection as “Data Identified but not Received” and directs users to a JPL point of contact who likely retired many years ago.

After exploratory conversations with senior colleagues, we acquired a digital copy of the Viking ionospheric profiles from Tamara Breus, first author of several articles that used these profiles (*Breus et al.*, 1998a,b).

5 Validation of electron density profiles supplied by Breus

5.1 Information supplied by Breus

The set of electron density profiles supplied by Breus contains 44 Viking Orbiter 1 profiles and 29 Viking Orbiter 2 profiles, a total of 73 profiles. The profiles cover solar zenith angles from 50 to 95 degrees and dates from 17 January 1977 to 20 August 1978. The profiles are summarized in Table 1.

Each profile supplied by Breus contains a set of values for electron density (ELECTRON_DENSITY) and altitude (Z_BREUS). On average, each profile contains about 70 data points. The vertical range of these profiles varies from profile to profile, but the median altitude of the highest data point is 250 km and the median altitude of the lowest data point is 90 km. The typical vertical resolution is 2 km, which is similar to the intrinsic resolution of the experiment (*Hinson et al.*, 1999).

Each profile is accompanied by the spacecraft identifier (i.e., Viking Orbiter 1 or 2) (SCT_ID_BREUS), orbit number for the relevant spacecraft (ORBIT_NUMBER_BREUS), year, month, and day of observation, solar zenith angle of observation (SZA_BREUS), and value of F10.7, a commonly-used solar irradiance proxy (F107_BREUS). Profiles are not labeled as either ingress or egress.

Due to the inclusion of two pairs of duplicate profiles (Section 5.3), the set of 73 profiles supplied by Breus contains 71 unique observations.

5.2 Validation against published images of profiles

Profiles supplied by Breus were visually compared against versions of these profiles in figures previously published in *Zhang et al.* (1990a) and *Kliore* (1992).

Profiles in *Zhang et al.* (1990a) are labeled by spacecraft, orbit number, and solar zenith angle. This is sufficient for us to match a profile in *Zhang et al.* (1990a) to its counterpart in the set supplied by Breus using SCT_ID_BREUS, ORBIT_NUMBER_BREUS, and SZA_BREUS. Of the 71 observations in the set of profiles supplied by Breus, 67 are shown in *Zhang et al.* (1990a). The omitted profiles are Viking Orbiter 1 observations on orbits 490, 508, and 523 and Viking Orbiter 2 observations on orbit 181. The figures of *Zhang et al.* (1990a) do not extend below 100 km altitude and hence do not show the full vertical range of the profiles.

Profiles in *Kliore* (1992) are labeled by solar zenith angle. For each panel of approximately ten profiles, the spacecraft and range of orbit numbers are stated. This is sufficient for us to match a profile in *Zhang et al.* (1990a) to its counterpart in the set supplied by Breus using SCT_ID_BREUS, ORBIT_NUMBER_BREUS, and SZA_BREUS. Of the 71 observations in the set of profiles supplied by Breus, 65 are shown in *Kliore* (1992). The omitted profiles are Viking Orbiter 1 observations on orbits 289 and 290 and Viking Orbiter 2 observations on orbits 149, 150, 151, and 181. The figures of *Kliore* (1992) do show the full vertical range of the profiles.

Only one profile in the set supplied by Breus is not shown by either *Zhang et al.* (1990a) or *Kliore* (1992): the profile from Viking Orbiter 2 orbit 181. As shown in the left panel of Figure 1, this profile is clearly unreliable. We advise data users to set aside this profile.

As illustrated in the right panel of Figure 1, the profiles supplied by Breus appear consistent with those shown in the figures of *Zhang et al.* (1990a) and *Kliore* (1992). As shown in Figure 2, the ionospheric peak densities and corresponding peak altitudes are also consistent

with previous publications (*Hantsch and Bauer, 1990*).

The most striking difference between the profiles supplied by Breus and those shown in the figures of *Zhang et al. (1990a)* and *Kliore (1992)* is that some profiles supplied by Breus extend to lower altitudes than shown by *Kliore (1992)*. For example, profiles from Viking Orbiter 1 orbits 609 and 676 and Viking Orbiter 2 orbits 174 and 176. The profile from Viking Orbiter 1 orbit 609 is labeled 70.6 in Figure 3a of *Kliore (1992)*. The profile from Viking Orbiter 1 orbit 676 is labeled 59.7 in Figure 3b of *Kliore (1992)*. The profile from Viking Orbiter 2 orbit 174 is labeled 88.7 in Figure 6 of *Kliore (1992)*. The profile from Viking Orbiter 2 orbit 176 is labeled 89.3 in Figure 6 of *Kliore (1992)*. Yet comparable low-altitude densities are shown by *Kliore (1992)* for several profiles, such as the profile from Viking Orbiter 2 orbit 507, which is labeled 85.4 in Figure 6 of *Kliore (1992)*. If Breus and Kliore used the same set of profiles, then it is unclear why low-altitude densities were omitted from some, but not all, profiles in *Kliore (1992)*. If Breus and Kliore used different sets of profiles, then it is unclear how the two sets are related and who modified one set to generate the other set (Section 6).

Densities reported at the lowest altitudes in profiles from Viking Orbiter 1 on orbits 289, 523, and 755 appear questionable, as shown in the left panel of Figure 3. At low altitudes below the main dayside ionospheric peak, densities usually decrease rapidly with decreasing altitude (*Withers, 2009*). Data users should treat data points that behave differently with caution.

Overall, we conclude that the profiles supplied by Breus are reasonably consistent with previous publications.

5.3 Instances of duplicate profiles

Two representations of the profile acquired by Viking Orbiter 1 on orbit 769 (26 July 1978, solar zenith angle of 61.30°) were supplied. Two representations of the profile acquired by Viking Orbiter 2 on orbit 149 (17 January 1977, solar zenith angle of 82.21°) were supplied. In each of these cases, the local filenames supplied by Breus imply that one representation

is primary (preferred) and one representation is secondary. These profiles are shown in Figure 4. The two representations are very similar for Viking Orbiter 1 on orbit 769, but markedly different for Viking Orbiter 2 on orbit 149.

The two representations for Viking Orbiter 1 on orbit 769 appear physically reasonable. The shape of the profile, peak electron density, and peak altitude are reasonable. Neither representation exhibits unusual behavior at either low or high altitudes. The fifth panel of Figure 9 of *Zhang et al.* (1990a) shows two profiles from Viking Orbiter 1 on orbit 769. These are the third and fourth profiles in the panel, both labeled 61. Based on the vertical extents and high-altitude density fluctuations, we judge that the third profile in the panel of *Zhang et al.* (1990a) is the secondary representation supplied by Breus and the fourth profile in the panel of *Zhang et al.* (1990a) is the primary representation supplied by Breus. Figure 3b of *Kliore* (1992) shows a profile from Viking Orbiter 1 on orbit 769 (profile labeled 61.4). Based on the presence of an M1 layer, a local density maximum around 180 km, and vertical extent above 250 km, we judge that the profile shown by *Kliore* (1992) is the primary representation supplied by Breus. Based on the available information, there is no compelling reason to reverse the original designations of primary and secondary. For Viking Orbiter 1 on orbit 769, we advise data users to use the primary representation and set aside the secondary representation.

The primary representation for Viking Orbiter 2 on orbit 149 does not exhibit unusual behavior at either low or high altitudes. However, it does not extend above 170 km. This upper boundary is relatively low, but is not a clear outlier with respect to other upper boundary altitudes in this set of profiles. This representation has a peak density of approximately $5 \times 10^4 \text{ cm}^{-3}$ and a peak altitude of approximately 110 km. This peak density value is consistent with other observations, but this peak altitude value is about 30 km smaller than typical for this solar zenith angle (Figure 2). The secondary representation for Viking Orbiter 2 on orbit 149 does not appear physically reasonable. Electron densities exceed $2 \times 10^4 \text{ cm}^{-3}$ at all altitudes below 100 km, which is inconsistent with other observations (*Withers*, 2009). The consistency of the vertical gradient in electron density from 0–100

km altitude to 200–300 km altitude suggests a possible uncorrected bias in the frequency data (e.g., *Dalba and Withers*, 2019). The secondary representation has a peak density of approximately $9 \times 10^4 \text{ cm}^{-3}$ and a peak altitude of approximately 140 km. This peak density value is large relative to other observations at similar solar zenith angles. It is on the edge of the distribution of observed values, but is not a clear outlier (Figure 2). This peak altitude value is consistent with other observations (Figure 2). The first panel of Figure 10 of *Zhang et al.* (1990a) shows two profiles from Viking Orbiter 2 on orbit 149. These are the first (labeled 81) and second (labeled 82) profiles in the panel. It is unclear why two representations of the same profile are labeled with different solar zenith angles. Based on their vertical extents and high-altitude density fluctuations, we judge that the first profile in the panel of *Zhang et al.* (1990a) is the primary representation supplied by Breus and the second profile in the panel of *Zhang et al.* (1990a) is the secondary representation supplied by Breus. *Kliore* (1992) does not show any profile from Viking Orbiter 2 on orbit 149.

The primary representation has an unrealistically low ionospheric peak altitude. The secondary representation has a peak density that is somewhat larger than expected, but it is not so large as to immediately invalidate the entire representation. However, densities between 0 km and 100 km are clearly unreasonably large and the existence of reported density values below 50 km is in itself a cause for concern. We are also mindful that *Kliore* (1992) did not show any profile from this orbit. *Kliore* may not have processed the raw radio science data to generate a set of ionospheric profiles for this mission, but he was sufficiently experienced to be able to critically evaluate a set of Viking Orbiter ionospheric profiles originally generated by his JPL colleague Fjeldbo and to identify severely flawed profiles. For Viking Orbiter 2 on orbit 149, we advise data users to set aside both the primary and secondary representations.

It is unclear why two representations exist for some observations. It is also unclear why two representations exist for these particular observations. It is possible that radio signals were acquired at two separate antennas, leading to one representation of the profile from each antenna (e.g., *Dalba and Withers*, 2019). It is possible that the data were reprocessed after,

e.g., improvements in the reconstructed trajectory (for instance, compare peak densities from Pioneer Venus Orbiter reported first by *Kliore et al.* (1979) then later by *Cravens et al.* (1981)). It is possible that some other explanation is valid. We are unable to resolve this puzzle. The only profiles shown in duplicate by *Zhang et al.* (1990a) are the only ones for which Breus supplied a secondary profile, which increases confidence that the set of profiles supplied by Breus is the same set as acquired by *Zhang et al.* (1990a) (Section 6).

5.4 Summary of validation activities

As described above, we set aside the profiles from Viking Orbiter 2 orbits 149 (both representations) and 181. We use the primary representation for Viking Orbiter 1 orbit 769 and set aside the secondary representation. This leaves a set of 69 acceptable profiles. Figures and numerical values in this document that are based on multiple profiles use the set of 69 acceptable profiles.

6 Provenance of electron density profiles supplied by Breus

When supplying this set of profiles to us, Breus stated that she received these data from the late Arv Kliore – but Kliore, who led almost every other radio occultation experiment flown, was not a member of the Viking radio science team. He was not a co-author on either *Fjeldbo et al.* (1977) or *Lindal et al.* (1979).

We deem it likely that Kliore received a copy of the dataset whilst contributing as a co-author to *Zhang et al.* (1990a). “The Viking mission radio occultation data,” said *Zhang et al.* (1990a), “from orbits 280–794 (Viking 1) and 149–508 (Viking 2) are on microfiche which are available from the investigators. The electron density profiles are given in the form of plotted altitude profiles, so that digital files were obtained by printing the plots and using a digitizer. Only dayside profiles with a distinct peak and acceptably low noise levels were

digitized.” Figures in *Zhang et al.* (1990a) show 41 ionospheric profiles for Viking Orbiter 1 from orbits 280 to 794 and 28 for Viking Orbiter 2 from orbits 149 to 508 and provide the orbit number and solar zenith angle for each profile. Breus provided us with 44 Viking Orbiter 1 profiles (all 41 shown by *Zhang et al.* (1990a) plus orbits 490, 508, and 523) and 29 Viking Orbiter 2 profiles (all 28 shown by *Zhang et al.* (1990a) plus orbit 181). Of the additional four profiles in the Breus data set, it is unclear why profiles from Viking Orbiter 1 orbits 490, 508, and 523 were excluded from publication in *Zhang et al.* (1990a). As shown in the right panel of Figure 3, they appear reasonable. We have been unable to solve this small puzzle, but do not think it is critical. Exclusion of the profile from Viking Orbiter 2 orbit 181 by *Zhang et al.* (1990a) is explained by its unusual characteristics, as discussed in Section 5.2. The evidence suggests that we have a complete copy of the dataset acquired by *Zhang et al.* (1990a) (Section 6).

Kliore was a co-author on practically all of post-Viking publications that used the Viking ionospheric profiles (*Zhang et al.*, 1990a,b; *Woo and Kliore*, 1991; *Kliore*, 1992; *Breus et al.*, 1998a,b; *Ness et al.*, 2000), while Zhang only participated in the three 1990 articles (*Hantsch and Bauer*, 1990; *Zhang et al.*, 1990a,b). (Note that Hantsch changed her name to Zhang in 1990.) This suggests that Kliore provided the profiles used in all relevant publications from 1991 onwards.

7 Uncertainties in electron density values

Uncertainties in measured electron density values are not stated in the original Viking-era publications. Nor are uncertainties included in the package supplied by Breus.

The standard method for determining uncertainties in electron density profiles measured by radio occultation experiments is to examine the portion of the derived electron density profile that extends to altitudes far above the top of ionosphere. The standard deviation of these high-altitude density values can be interpreted as the experimental uncertainty in all electron density values from that specific profile. We are unable to apply this method to the

set of profiles supplied by Breus as these profiles do not extend to high enough altitudes. It is unlikely that the original observations ceased at 250 km altitude, so presumably the profiles were truncated at some stage during the data processing. For instance, the experimenters may have scanned up/down from the ionospheric peak, then truncated the profiles when electron density values first dropped below the threshold at which they felt confident in the derived electron density values.

We investigated various possible methods for assigning uncertainties to reported electron density values. We examined the smallest value of electron density reported for each profile ($Nmin$), the highest-altitude value of electron density reported for each profile ($Ntop$), and the standard deviation of the five highest-altitude electron density values in each profile ($SDEV5$). We also performed a linear fit to the dependence of electron density on altitude using the five highest-altitude electron density values in each profile, then examined the root-mean-square of the difference between these data points and the fit ($RMS5$). These quantities are shown in Figure 5. The set of $Nmin$ values has a mean of 1400 cm^{-3} and standard deviation of 1300 cm^{-3} . The set of $Ntop$ values has a mean of 2800 cm^{-3} and standard deviation of 2300 cm^{-3} . The set of $SDEV5$ values has a mean of 1800 cm^{-3} and standard deviation of 1300 cm^{-3} . The set of $RMS5$ values has a mean of 900 cm^{-3} and standard deviation of 700 cm^{-3} . Based on this cursory analysis, we judge that a reasonable estimate for the characteristic electron density uncertainty in these profiles is 2000 cm^{-3} .

8 Ancillary information

It is necessary to validate the ancillary information supplied by Breus (SCT_ID_BREUS, ORBIT_NUMBER_BREUS, SZA_BREUS, F107_BREUS and year, month, and day of observation). Tables in *Lindal et al. (1979)* and *Ness et al. (2000)* were useful for assessing the ancillary information. Table 1 of *Lindal et al. (1979)* lists spacecraft, orbit number, ingress or egress, latitude, and longitude for many ingress and egress occultations by Viking Orbiters 1 and 2. Table 2 of *Ness et al. (2000)* lists orbit number, latitude, longitude, and solar zenith

angle for a subset of 17 Viking 1 ingress occultations.

It is also necessary to generate additional ancillary information to support the analysis and interpretation of these ionospheric observations, including the time of the observation, areocentric latitude, areocentric east longitude, local solar time, Ls, and whether the observation was ingress or egress. We used the SPICE trajectory kernels for Viking Orbiters 1 and 2 (<http://naif.jpl.nasa.gov/pub/naif/VIKING/kernels/>) to find the times and locations of each occultation point. The occultation point was defined as the time and location where the ray path of the radio signal transmitted from the spacecraft to Earth has a closest approach distance to Mars equal to the representative ionospheric radial distance of 3550 km. Specifically, we found date and time (OCC_TIME_SPICE), solar zenith angle (SZA_SPICE), areocentric latitude (LAT_SPICE), areocentric east longitude (LON_SPICE), local solar time (LST_SPICE), and Ls (LS_SPICE). Throughout this document, we use our SPICE-derived time and location information in preference to similar information from other sources.

We matched each profile in the set supplied by Breus to an occultation opportunity found by SPICE. For each profile in the set supplied by Breus, we identified each occultation opportunity found by SPICE on the corresponding date. As the orbital periods of the Viking Orbiters were approximately 24 hours, there was generally one ingress occultation and one egress occultation on a given day. Discrimination between ingress and egress was based upon the solar zenith angle supplied by Breus. Potential ambiguities were resolved by comparing latitudes and longitudes between output from SPICE (areocentric) and values in Table 1 of *Lindal et al. (1979)*.

As expected, most profiles in the set supplied by Breus corresponded to ingress occultations. Egress occultations were conducted in a low-accuracy one-way mode in which frequency was referenced to the imperfect spacecraft oscillator, whereas ingress occultations were conducted in a higher-accuracy two-way mode in which frequency was referenced to a more stable ground-based oscillator at the Deep Space Network station (*Fjeldbo et al., 1977; Lindal et al., 1979*). However, profiles from Viking Orbiter 2 on orbits 225, 227, and 229 were unexpectedly found to correspond to egress observations.

These profiles are shown in Figure 6. For the profile from Viking Orbiter 2 on orbit 225, Breus identified the date as 8 April 1977 and the solar zenith angle as 85.4° . On this date, SPICE identified an ingress occultation at -41.41° areocentric latitude, -67.12° areocentric east longitude, and solar zenith angle of 107.36° , as well as an egress occultation at 64.04° areocentric latitude, 157.22° areocentric east longitude, and solar zenith angle of 85.41° . For Viking Orbiter 2 on orbit 225, *Lindal et al.* (1979) reported an ingress occultation at -40.58° latitude and -68.26° longitude, as well as an egress occultation at 64.57° latitude and 161.11° longitude. The three values of peak electron density are 4.3×10^4 , 5.9×10^4 , and $3.7 \times 10^4 \text{ cm}^{-3}$ respectively. These values are consistent with previous observations at the solar zenith angle of the egress occultation, but are appreciably larger than previous observations at the solar zenith angle of the ingress occultation (*Hantsch and Bauer, 1990; Zhang et al., 1990b*). We conclude that these three profiles were acquired on egress occultation opportunities. Note that Figure 10 of *Zhang et al.* (1990a) labels them as ingress occultations.

As this example shows, minor discrepancies exist between output from SPICE and the solar zenith angles supplied by Breus and the latitudes and longitudes tabulated by *Lindal et al.* (1979). We consider these acceptable considering differences in software and evolution of the reconstructed Viking trajectory. No major discrepancies between these quantities were identified.

Regarding F107_BREUS, it is clear from their magnitudes that the F10.7 values supplied by Breus are valid at the orbital distance of Earth, not Mars. It is not clear whether these F10.7 values are valid at the instantaneous orbital distance of Earth (i.e., observed) or at 1 AU (i.e., adjusted). In either case, data users are advised to set aside the F10.7 values supplied by Breus and instead use suitable solar irradiance proxies from verifiable sources.

9 Definition of altitude

Electron density in the profiles supplied by Breus is reported as a function of altitude. Definitions of altitude on Mars have changed significantly since the Viking era (*Withers*

and Jakosky, 2017). Treating Viking-era altitudes as equivalent to MOLA-era altitudes can introduce errors on the order of 5 km, half a scale height.

Zhang et al. (1990a) stated that “the altitudes were corrected for local topography by subtracting the 6.1 mbar reference radius given on the microfiche from the radius given on the plot.” That is, the original data products were reported as a function of radial distance from the planet’s center of mass, which is a common and sensible approach for radio occultation data. *Zhang et al.* (1990a) subtracted the stated 6.1 mbar reference radius from each of the radial distances listed in the electron density profile in order to convert the radial distances into altitudes.

In order for these profiles to have an unambiguous vertical reference, it is therefore necessary to reverse the “radial distance to altitude” conversion of *Zhang et al.* (1990a), which requires specification of the 6.1 mbar reference surface.

Lindal et al. (1979) cites several sources that describe this reference surface in quantitative terms. However, most of these source describe the gravity field or topography, not the reference surface. We adopt the triaxial ellipsoid representation of the 6.1 mbar reference surface reported by *Cain et al.* (1973) from Mariner 9 observations. The position coordinates x , y , z of this surface satisfy:

$$\left(\frac{x}{a}\right)^2 + \left(\frac{y}{b}\right)^2 + \left(\frac{z}{c}\right)^2 = 1 \quad (1)$$

where the origin is at the center of mass of Mars, the z axis is the rotation axis, the x axis points an angle θ west of the prime meridian, and the y axis completes the right-handed set, a is 3396.67 km, b is 3395.23 km, c is 3377.22 km, and θ is 108.1 degrees.

We use our SPICE-derived areocentric latitudes and areocentric east longitudes, the standard relationships between cartesian and spherical polar coordinates, and Equation 1 to find the radial distance of the 6.1 mbar reference surface (RREF_61MBAR) appropriate for each profile. We add the value of RREF_61MBAR to each value of altitude reported in that profile (Z_BREUS) to obtain a corresponding set of radial distances (RADIAL_DISTANCE). In principle, these values should match those on the microfiche exam-

ined by *Zhang et al.* (1990a). However, it is not possible to verify this directly. Next, we use our SPICE-derived areocentric latitudes and areocentric east longitudes to find the radial distance of the MOLA reference surface (RREF_MOLA) appropriate for each profile. Specifically, we find the radius of the MOLA areoid from the 4 pixel per degree MOLA Mission Experiment Gridded Data Record (MEGDR) that is available online at <http://pds-geosciences.wustl.edu/missions/mgs/megdr.html>. Finally, we subtract RREF_MOLA from each value of RADIAL_DISTANCE in that profile to obtain a corresponding set of MOLA altitudes (Z_MOLA). Throughout this document, we use MOLA altitudes (Z_MOLA) instead of the altitudes supplied by Breus (Z_BREUS) unless explicitly stated otherwise.

10 Completeness of set of profiles supplied by Breus

Is the set of profiles supplied by Breus complete? Its 73 profiles contain 71 unique observations, of which 43 are Viking Orbiter 1 ingress profiles, 25 are Viking Orbiter 2 ingress profiles, and 3 are Viking Orbiter 2 egress profiles. There are no Viking Orbiter 1 egress profiles. All profiles shown by *Zhang et al.* (1990a) and *Kliore* (1992) are included in the set of profiles supplied by Breus.

However, Table 1 of *Lindal et al.* (1979) lists 99 ingress and 14 egress occultations by Viking Orbiter 1 and 33 ingress and 9 egress occultations by Viking Orbiter 2. 132 ingress occultations and 23 egress occultations are listed for a total of 155. Of the set of profiles supplied by Breus, Viking Orbiter 1 ingress profiles on orbits 280, 490, and 745 and Viking Orbiter 2 ingress profiles on orbits 464, 465, 506, and 507 are not listed by *Lindal et al.* (1979).

Lindal et al. (1979) lists 59 Viking Orbiter 1 ingress occultations, 14 Viking Orbiter 1 egress occultations, 12 Viking Orbiter 2 ingress occultations, and 20 Viking Orbiter 2 egress occultations that are not in the set supplied by Breus.

Of these 59 Viking Orbiter 1 ingress occultations, 20 are from orbits 108 to 132, 21 are from orbits 311 to 392, and 15 are from orbits 492 to 574. The remaining three are from orbits

685, 749, and 796. Observations from Viking Orbiter 1 orbits 108 to 132 are of low quality. These profiles were acquired when Mars was within 14 degrees of superior conjunction (Mars directly behind the Sun as seen from Earth). “Because of phase scintillation in the solar corona the noise level was considerably higher than that seen in previous experiments” (*Fjeldbo et al.*, 1977). This also explains why *Fjeldbo et al.* (1977) did not show any profiles from these occultations. Observations from ingress occultations on Viking Orbiter 1 orbits 311 to 392 and 492 to 574 are at nightside solar zenith angles (*Zhang et al.*, 1990b). Nightside solar zenith angles were confirmed using SPICE. Observations from ingress occultations on Viking Orbiter 1 orbits 685, 749, and 796 are within a set of observations that were supplied by Breus (see Table 1). Solar zenith angles were firmly on the dayside on missing observations. It is unclear why these observations are not in the set supplied by Breus. They were not shown by *Zhang et al.* (1990a) either.

Of these 12 Viking Orbiter 2 ingress occultations, 7 are from orbits 213 to 271 and 4 are from orbits 486 to 490. The remaining one are from orbit 182. Observations from ingress occultations on Viking Orbiter 2 orbits 182, 213 to 271, and 486 to 490 are at nightside solar zenith angles (*Zhang et al.*, 1990b).

Most of the ingress profiles that are listed by *Lindal et al.* (1979), but are not included in the set supplied by Breus, are omitted from the set supplied by Breus due to either solar conjunction or nightside solar zenith angles. Three ingress profiles listed by *Lindal et al.* (1979) (Viking Orbiter 1 orbits 685, 749, and 796) are omitted from the set supplied by Breus for unknown reasons. They are not shown in figures in *Zhang et al.* (1990a) or *Kliore* (1992). It is possible that data quality was degraded on these observations. Egress profiles that are listed by *Lindal et al.* (1979), but are not included in the set supplied by Breus, are omitted from the set supplied by Breus due to poor data quality in the one-way observing mode and/or nightside solar zenith angles. We conclude that the set of profiles supplied by Breus contains the complete set of high quality, dayside electron density profiles from Viking Orbiters 1 and 2.

11 Overview of electron density measurements

The temporal and solar zenith angle coverage of the profiles is shown in the left panel of Figure 7. The geographical coverage of the profiles is shown in the right panel of Figure 7. Selected profiles are shown in Figure 8 for solar zenith angles near 50° , 60° , 70° , 80° , and 90° . The left panel uses a linear scale for electron density, whereas the right panel uses a logarithmic scale for electron density. Different features are highlighted by the different scales: a linear scale highlights the main peak, a logarithmic scale highlights the topside. The left panel shows the peak density decreasing and peak altitude increasing with increasing solar zenith angle, as expected. The right panel shows that topside structure, which is often well-represented by an exponential decrease in electron density with increasing altitude, is markedly less controlled by solar zenith angle. As can be seen in Figure 2 (and was previously shown by *Hantsch and Bauer (1990)*), ionospheric peak altitude increases sharply as solar zenith angle increases through 90° .

The dependence of electron density on altitude and solar zenith angle is shown in the left panel of Figure 9. Each pixel indicates the average value of electron density within a region of five degrees extent in solar zenith angle and five km extent in altitude. The decrease in electron density from dayside to nightside is readily apparent. The increase in peak altitude with increasing solar zenith angle can also be seen.

At most altitudes, dayside electron density decreases appreciably with increasing solar zenith angle. This is apparent in the left panel of Figure 9 around 120 km and 240 km altitude, for instance. However, dayside electron density appears almost independent of solar zenith angle at intermediate altitudes such as 160 km and 200 km, as highlighted in the right panel of Figure 9. This behavior can also be seen in Figure 8.

Below ~ 200 km, the ionosphere is in photochemical equilibrium. In an idealized photochemical equilibrium (e.g., Equation 2 of *Withers (2009)*), electron density decreases with increasing solar zenith angle at altitudes around the ionospheric peak, but is practically independent of solar zenith angle far above the ionospheric peak. This explains the trends seen at 120 km, 160 km, and 200 km altitude. The observed behavior at 240 km altitude is

not consistent with the idealized photochemical equilibrium prediction. Here the ionosphere is not in photochemical equilibrium. Instead, the behavior at 240 km likely results from plasma transport processes and interactions with the surrounding space environment.

12 Archive organization and naming

This section describes the basic organization of this archive, and the naming conventions used for the bundle, collection, and product logical identifiers.

12.1 Logical identifiers

Every product in PDS is assigned an identifier which allows it to be uniquely identified across the system. This identifier is referred to as a Logical Identifier or LID. A LIDVID (Versioned Logical Identifier) includes product version information, and allows different versions of a specific product to be referenced uniquely. A product's LID and VID are defined as separate attributes in the product label. LIDs and VIDs are assigned by the entity generating the labels and are formed according to the conventions described in Sections 12.1.1 and 12.1.2 below. The uniqueness of a product's LIDVID may be verified using the PDS Registry and Harvest tools.

12.1.1 LID formation

LIDs take the form of a Uniform Resource Name (URN). LIDs are restricted to ASCII lower case letters, digits, dash, underscore, and period. Colons are also used, but only to separate prescribed components of the LID. Within one of these prescribed components dash, underscore, or period are used as separators. LIDs are limited in length to 255 characters.

LIDs for products in this archive are formed according to the following conventions:

Bundle LIDs are formed by appending a bundle-specific ID to the base ID:

`urn:nasa:pds:<bundle ID>`

Since all PDS bundle LIDs are constructed this way, this bundle-specific ID must be unique across all bundles archived with the PDS.

Collection LIDs are formed by appending a collection-specific ID to the collection's parent bundle LID:

```
urn:nasa:pds:<bundle ID>:<collection ID>
```

Since the collection LID is based on the bundle LID, which is unique across PDS, the only additional condition is that the collection ID must be unique across the bundle. Collection IDs correspond to the collection type (e.g. “**browse**”, “**data**”, “**document**”, etc.). Additional descriptive information may be appended to the collection type (e.g. “**data-raw**”, “**data-calibrated**”, etc.) to ensure that multiple collections of the same type within a single bundle have unique LIDs.

Basic product LIDs are formed by appending a product specific ID to the product's parent collection LID:

```
urn:nasa:pds:<bundle ID>:<collection ID>:<product ID>
```

Since the product LID is based on the collection LID, which is unique across PDS, the only additional condition is that the product ID must be unique across the collection.

12.1.2 VID formation

Product version ID's consist of major and minor components separated by a “.” (M.n). Both components of the VID are integer values. The major component is initialized to a value of “1”, and the minor component is initialized to a value of “0”. The minor component resets to “0” when the major component is incremented.

12.2 Archive contents for the voroelden bundle

The Viking Orbiters 1 and 2 Radio Occultation Electron Density archive contains one bundle:

```
urn:nasa:pds:voroelden
```

There are two collections in this bundle:

```
urn:nasa:pds:voroelden:data_derived (a data collection)
```

`urn:nasa:pds:voroelden:document` (a document collection).

Product LIDs for a given collection are given in the portion of Section 12.2 that describes that collection. The following sections describe the contents of this bundle in greater detail.

12.2.1 `voroelden:data_derived` data collection

The `voroelden:data_derived` data collection contains one distinct type of product: Mars ionospheric electron density profiles from occultations. The generation and validation of this type of products is discussed earlier in this document.

12.2.2 Description of electron density data products

Electron density data products contain vertical profiles of the electron density in the ionosphere of Mars during an occultation. They are ASCII files.

The file naming convention is:

`voroelden_d_eee_f_vxx_rxx.csv`

where:

d: 1 for Viking Orbiter 1, 2 for Viking Orbiter 2

eee: Orbit number for relevant spacecraft

f: **a** for primary representation supplied by Breus for this observation, **b** for secondary representation supplied by Breus for this observation (see Section 5 for further discussion)

vxx: identifies the major component **xx** of the version number of this product

rxx: identifies the minor component **xx** of the version number of this product

csv: indicates that this data product is a comma-separated file

The product LID for this file is:

`voroelden_d_eee_f`

A sample product LID for an electron density data product is: `voroelden_1_280_a`.

12.2.3 voroelden:document document collection

The `voroelden:document` document collection contains one distinct type of product: the user guide you are currently reading. This is a PDF/A document originally written in LaTeX.

The file naming convention is:

`userguide_vxx_rxx.pdf`

where

`vxx`: identifies the major component `xx` of the version number of this product

`rxx`: identifies the minor component `xx` of the version number of this product

The product LID for this file is:

`userguide`

Hence the complete LID is:

`urn:nasa:pds:voroelden:document:userguide`

13 Archive product formats

This section describes the format of each type of product in this archive.

The products that comprise this archive are formatted in accordance with PDS specifications, specifically: Planetary Data System Standards Reference, Version 1.8.0, 21 March 2017; PDS4 Data Dictionary — Abridged, Version 1.8.0.0, 10 March 2017; and Planetary Data System (PDS) PDS4 Information Model Specification, 1.8.0.0, 10 March 2017.

13.1 Data file formats

This section describes the format and record structure of the electron density data product. These products are archived as PDS4 Table_Delimited objects. They are ASCII files. They are stored as comma-separated files and have the extension `.csv`.

Each electron density data product contains two tables. The first table is a header that contains 12 columns. It has one row.

Column 1: OCC_TIME_SPICE. Dimensionless. UTC at Mars at time of occultation, as found from SPICE.

Column 2: SCT_ID_BREUS. Dimensionless. ASCII_Integer. Identifier of spacecraft: “1” for Viking Orbiter 1, “2” for Viking Orbiter 2, as provided by Breus.

Column 3: ORBIT_NUMBER_BREUS. Dimensionless. ASCII_Integer. Orbit number for relevant spacecraft at time of occultation, as provided by Breus.

Column 4: SZA_BREUS. Unit=degree. ASCII_Real. Solar zenith angle at time and location of occultation, as provided by Breus.

Column 5: SZA_SPICE. Unit=degree. ASCII_Real. Solar zenith angle at time and location of occultation, as found from SPICE.

Column 6: LAT_SPICE. Unit=degree. ASCII_Real. Areocentric north latitude at time and location of occultation, as found from SPICE.

Column 7: LON_SPICE. Unit=degree. ASCII_Real. Areocentric east longitude at time and location of occultation, as found from SPICE.

Column 8: LST_SPICE. Unit=hour. ASCII_Real. Local solar time at time and location of occultation, as found from SPICE.

Column 9: LS_SPICE. Unit=degree. ASCII_Real. Areocentric east longitude of the Sun (Ls) at time and location of occultation, as found from SPICE.

Column 10: RREF_61MBAR. Unit=km. ASCII_Real. Radial distance to 6.1 mbar equipotential surface at location of occultation.

Column 11: RREF_MOLA. Unit=km. ASCII_Real. Radial distance to MOLA equipotential surface at location of occultation.

Column 12: F107_BREUS. Dimensionless. ASCII_Real. Value of F10.7 solar irradiance proxy at Earth at time of occultation, as provided by Breus.

The second table contains the electron density and altitude values. It has four altitude-ordered columns and a variable number of rows. The typical number of rows is approximately 70.

Column 1: Z_BREUS. Unit=km. ASCII_Real. Altitude of measurement relative to 6.1

mbar equipotential surface at location of occultation, as provided by Breus.

Column 2: Z_MOLA. Unit=km. ASCII_Real. Altitude of measurement relative to MOLA equipotential surface at location of occultation.

Column 3: RADIAL_DISTANCE. Unit=km. ASCII_Real. Radial distance of measurement.

Column 4: ELECTRON_DENSITY. Unit= cm^{-3} . ASCII_Real. Electron density measurement.

13.2 PDS labels

PDS labels are ASCII text files written in the eXtensible Markup Language (XML). All product labels are detached from the digital files (if any) containing the data objects they describe (except Product_Bundle). There is one label for every product. Each product, however, may contain one or more data objects. The data objects of a given product may all reside in a single file, or they may be stored in multiple separate files. PDS4 label files must end with the file extension “.xml”.

For this archive, PDS labels will conform to the PDS master schema based upon version 1.8.0.0 of the PDS information model for structure and version 1.8.0.0 of the PDS schematron for content. By use of an XML editor these documents may be used to validate the structure and content of the product labels. A list of the XML documents associated with this archive is included in the XML_Schema collection section for each bundle.

14 Summary

We have recovered, validated, and archived the complete set of high quality, dayside electron density profiles from Viking Orbiters 1 and 2.

The archived profiles are accompanied by useful ancillary information that includes date and time, solar zenith angle, areocentric latitude, areocentric east longitude, local solar time, and Ls. These values were found directly from the Viking Orbiters 1 and 2 SPICE kernel.

Several related vertical coordinates are archived: altitudes relative to a 6.1 mbar reference surface (as supplied by Breus), altitude relative to a MOLA reference surface, and radial distance.

73 profiles were supplied by Breus. We deem 69 of them to be acceptable for scientific analysis. Four profiles were deemed not to be acceptable for scientific analysis. The profile from Viking Orbiter 2 orbit 181 is clearly unreliable. The secondary representation from Viking Orbiter 1 orbit 769 is redundant. Both the primary and the secondary representations from Viking Orbiter 2 orbit 149 are unreliable.

Relative to the widely-used set of radio occultation electron density profiles from MGS, these Viking profiles have better sensitivity, higher vertical extent, more global coverage, and greater solar zenith angle coverage. They are ready for use in scientific investigations of the ionosphere of Mars and related topics.

15 Acknowledgements

This work was supported, in part, by NASA award NNX16AG45G. Substantial contributions to the generation and validation of these data products were made by Marianna Felici, Casey Flynn, and Marissa Vogt (Boston University). We thank Greg Neumann and colleagues for advice concerning representations of the 6.1 mbar surface and the NSSDC for supplying Viking Orbiter radio science frequency data (PSPG-00406) for evaluation. We also thank Tamara Breus, Martina Zhang, Janet Luhmann, Arv Kliore, and other colleagues responsible for the storage and transfer of these data products from the original experimenters to us over a period of four decades.

16 References

References

- Breus, T. K., K. Y. Pimenov, M. N. Izakov, A. M. Krymskii, J. G. Luhmann, and A. J. Kliore (1998a), Conditions in the Martian ionosphere/atmosphere from a comparison of a thermospheric model with radio occultation data, *Planet. Space Sci.*, *46*, 367–376, doi:10.1016/S0032-0633(97)00168-2.
- Breus, T. K., K. Y. Pimenov, J. G. Luhmann, A. Krymsky, T. Hagfors, W. I. Axford, and A. Kliore (1998b), Application of Viking radio occultation data to the future studies of the Martian ionosphere, *Adv. Space Res.*, *22*, 463–470, doi:10.1016/S0273-1177(98)00087-8.
- Cain, D. L., A. J. Kliore, B. L. Seidel, M. J. Sykes, and P. Woiceshyn (1973), Approximations to the mean surface of Mars and Mars atmosphere using Mariner 9 occultations., *J. Geophys. Res.*, *78*, 4352–4354, doi:10.1029/JB078i020p04352.
- Chen, R. H., T. E. Cravens, and A. F. Nagy (1978), The martian ionosphere in light of the Viking observations, *J. Geophys. Res.*, *83*, 3871–3876.
- Cravens, T. E., J. U. Kozyra, A. F. Nagy, and A. J. Kliore (1981), The ionospheric peak on the Venus dayside, *J. Geophys. Res.*, *86*, 11,323–11,329.
- Dalba, P. A., and P. Withers (2019), Cassini Radio Occultation Observations of Titan’s Ionosphere: The Complete Set of Electron Density Profiles, *J. Geophys. Res.*, *124*(1), 643–660, doi:10.1029/2018JA025693.
- Fjeldbo, G., D. Sweetnam, J. Brenkle, E. Christensen, D. Farless, J. Mehta, B. Seidel, W. Michael, Jr., A. Wallio, and M. Grossi (1977), Viking radio occultation measurements of the Martian atmosphere and topography — Primary mission coverage, *J. Geophys. Res.*, *82*, 4317–4324, doi:10.1029/JS082i028p04317.

- Hantsch, M. H., and S. J. Bauer (1990), Solar control of the Mars ionosphere, *Planet. Space Sci.*, *38*, 539–542.
- Hinson, D. P., R. A. Simpson, J. D. Twicken, G. L. Tyler, and F. M. Flasar (1999), Initial results from radio occultation measurements with Mars Global Surveyor, *J. Geophys. Res.*, *104*, 26,997–27,012.
- Hunten, D. M., L. Colin, T. M. Donahue, and V. I. Moroz (1983), *Venus*, Univ. Arizona Press, Arizona.
- Kieffer, H. H., B. M. Jakosky, C. W. Snyder, and M. S. Matthews (1992), *Mars*, Univ. Arizona Press, Arizona.
- Kliore, A. J. (1992), Radio occultation observations of the ionospheres of Mars and Venus, in *Venus and Mars: Atmospheres, ionospheres, and solar wind interactions*, *Geophysical Monograph Series*, vol. 66, pp. 265–276, American Geophysical Union, Washington, DC.
- Kliore, A. J., I. R. Patel, A. F. Nagy, T. E. Cravens, and T. I. Gombosi (1979), Initial observations of the nightside ionosphere of Venus from Pioneer Venus Orbiter radio occultations, *Science*, *205*, 99–102.
- Lindal, G. F., H. B. Hotz, D. N. Sweetnam, Z. Shippony, J. P. Brenkle, G. V. Hartsell, and R. T. Spear (1979), Viking radio occultation measurements of the atmosphere and topography of Mars - Data acquired during 1 Martian year of tracking, *J. Geophys. Res.*, *84*, 8443–8456, doi:10.1029/JB084iB14p08443.
- Mutch, T. A. (1980), Introduction to Pioneer Venus Special Issue, *J. Geophys. Res.*, *85*, 7573–7573, doi:10.1029/JA085iA13p07573.
- Ness, N. F., M. H. Acuña, J. E. P. Connerney, A. J. Kliore, T. K. Breus, A. M. Krymskii, P. Cloutier, and S. J. Bauer (2000), Effects of magnetic anomalies discovered at Mars on the structure of the martian ionosphere and solar wind interaction as follows from radio occultation experiments, *J. Geophys. Res.*, *105*, 15,991–16,004, doi:10.1029/1999JA000212.

- Snyder, C. W., and V. I. Moroz (1992), Spacecraft exploration of Mars., in *Mars*, edited by H. H. Kieffer, B. M. Jakosky, C. W. Snyder, and M. S. Matthews, pp. 71–119, Univ. Arizona Press, Arizona.
- Soffen, G. A. (1977), The Viking project, *J. Geophys. Res.*, *82*, 3959–3970, doi:10.1029/JS082i028p03959.
- Withers, P. (2009), A review of observed variability in the dayside ionosphere of Mars, *Adv. Space Res.*, *44*, 277–307, doi:10.1016/j.asr.2009.04.027.
- Withers, P. (2010), Prediction of uncertainties in atmospheric properties measured by radio occultation experiments, *Adv. Space Res.*, *46*, 58–73, doi:10.1016/j.asr.2010.03.004.
- Withers, P., and B. M. Jakosky (2017), Implications of MAVEN’s planetographic coordinate system for comparisons to other recent Mars orbital missions, *J. Geophys. Res.*, *122*, 802–807, doi:10.1002/2016JA023470.
- Withers, P., S. Weiner, and N. R. Ferreri (2015), Recovery and validation of Mars ionospheric electron density profiles from Mariner 9, *Earth, Planets, and Space*, *67*, 194, doi:10.1186/s40623-015-0364-2.
- Woo, R., and A. J. Kliore (1991), Magnetization of the ionospheres of Venus and Mars: Results from radio occultation measurements, *J. Geophys. Res.*, *96*, 11,073–11,081, doi:10.1029/91JA00313.
- Zhang, M. H. G., J. G. Luhmann, and A. J. Kliore (1990a), An observational study of the nightside ionospheres of Mars and Venus with radio occultation methods, *J. Geophys. Res.*, *95*, 17,095–17,102, doi:10.1029/JA095iA10p17095.
- Zhang, M. H. G., J. G. Luhmann, A. J. Kliore, and J. Kim (1990b), A post-Pioneer Venus reassessment of the martian dayside ionosphere as observed by radio occultation methods, *J. Geophys. Res.*, *95*, 14,829–14,839.

17 Tables

Table 1: Summary of Viking Orbiters 1 and 2 electron density profiles. Latitudes and longitudes are areocentric. Superscripts are as follows. a — Spacecraft, 1 for Viking Orbiter 1 and 2 for Viking Orbiter 2. b — Solar zenith angle. c — Local solar time. d — Peak electron density. e — Peak altitude. p — If duplicate representations exist, then primary representation. s — If duplicate representations exist, then secondary representation. w — Egress occultation (if omitted, then ingress occultation). x — Assessed to be unreliable.

Time (UTC at Mars)	Sct ^a	Orbit	SZA ^b (degrees)	Latitude (°N)	Longitude (°E)	LST ^c (hrs)	Ls (degrees)	N_{max}^d (cm ⁻³)	z_{max}^e (km)
1977-03-26T20:18:10	1	280	79.78	-44.88	-85.33	5.72	228.92	7.0E+04	150.5
1977-04-04T15:47:57	1	289	86.84	-60.97	39.34	3.80	234.46	6.4E+04	160.1
1977-04-05T15:17:59	1	290	87.58	-61.98	52.22	3.52	235.08	3.2E+04	178.2
1977-04-07T14:18:37	1	292	89.03	-63.52	77.29	2.93	236.32	2.9E+04	162.8
1977-10-20T17:47:20	1	490	49.71	-19.83	-141.15	8.79	352.22	1.4E+05	118.5
1977-11-07T17:26:14	1	508	51.60	-24.42	37.62	8.89	1.29	1.3E+05	122.6
1977-11-22T17:01:19	1	523	55.11	-27.87	-173.36	8.86	8.65	1.6E+05	120.1

1978-01-15T15:01:09	1	577	94.31	37.73	164.91	19.11	33.93	1.6E+04	159.8
1978-02-01T14:36:46	1	594	80.81	38.52	-42.31	18.08	41.60	8.0E+04	136.0
1978-02-16T14:12:49	1	609	70.64	38.56	95.17	17.30	48.27	9.6E+04	130.8
1978-02-17T14:10:33	1	610	70.06	38.52	104.62	17.26	48.72	9.7E+04	133.0
1978-02-19T14:05:35	1	612	68.93	38.42	123.65	17.17	49.60	9.5E+04	131.6
1978-02-24T13:57:09	1	617	66.32	38.00	170.52	16.98	51.81	1.2E+05	127.5
1978-03-01T13:55:04	1	622	64.01	37.57	-143.75	16.80	54.01	1.2E+05	132.3
1978-03-04T13:50:56	1	625	62.78	37.36	-115.42	16.71	55.33	1.2E+05	131.4
1978-03-05T13:49:05	1	626	62.39	37.24	-105.84	16.69	55.77	1.2E+05	130.4
1978-03-18T13:26:36	1	639	58.21	35.19	19.37	16.38	61.46	1.4E+05	122.3
1978-04-16T12:45:46	1	668	53.56	27.93	-58.68	16.00	74.11	1.4E+05	122.3
1978-04-17T12:43:48	1	669	53.48	27.61	-48.76	15.99	74.55	1.3E+05	122.4
1978-04-18T12:41:51	1	670	53.42	27.30	-38.83	15.98	74.99	1.3E+05	123.2
1978-04-24T12:32:18	1	676	53.10	25.37	20.28	15.93	77.60	1.4E+05	124.3
1978-05-07T12:12:29	1	689	52.92	20.74	148.35	15.84	83.29	1.5E+05	120.7
1978-05-09T12:07:22	1	691	52.95	20.03	168.59	15.83	84.16	1.4E+05	125.6
1978-05-13T12:02:40	1	695	53.04	18.47	-152.30	15.80	85.92	1.4E+05	128.2
1978-05-31T11:39:33	1	713	54.07	11.11	24.33	15.69	93.86	1.4E+05	118.8
1978-06-24T11:09:04	1	737	56.64	0.770	-99.92	15.55	104.58	1.4E+05	127.2
1978-06-25T11:08:47	1	738	56.77	0.340	-90.33	15.54	105.04	1.0E+05	123.8

1978-07-02T10:59:17	1	745	57.71	-2.760	-21.36	15.51	108.21	9.9E+04	126.4
1978-07-12T10:43:34	1	755	59.14	-7.060	77.85	15.47	112.78	1.4E+05	127.3
1978-07-15T10:41:42	1	758	59.59	-8.350	106.93	15.46	114.16	1.4E+05	124.1
1978-07-23T10:27:41	1	766	60.83	-11.83	-173.27	15.43	117.86	1.2E+05	122.8
1978-07-24T10:24:47	1	767	60.99	-12.25	-163.00	15.43	118.32	1.2E+05	126.3
1978-07-25T10:22:05	1	768	61.14	-12.67	-152.78	15.42	118.79	1.1E+05	125.3
1978-07-26T10:19:47	1	769 ^p	61.30	-13.10	-142.66	15.42	119.26	1.2E+05	119.6
1978-07-29T10:16:24	1	772	61.77	-14.31	-113.11	15.42	120.66	1.3E+05	126.4
1978-07-30T10:16:14	1	773	61.93	-14.72	-103.49	15.42	121.13	1.2E+05	131.4
1978-07-31T10:16:15	1	774	62.09	-15.13	-93.92	15.41	121.60	1.2E+05	128.6
1978-08-03T10:15:48	1	777	62.56	-16.33	-65.05	15.41	123.01	1.2E+05	124.4
1978-08-04T10:15:09	1	778	62.72	-16.74	-55.31	15.41	123.48	1.1E+05	120.8
1978-08-14T09:57:03	1	788	64.35	-20.77	45.09	15.41	128.23	1.1E+05	122.4
1978-08-16T09:53:37	1	790	64.65	-21.44	65.22	15.42	129.19	1.1E+05	125.6
1978-08-18T09:51:08	1	792	64.98	-22.18	85.09	15.42	130.15	8.2E+04	124.5
1978-08-20T09:49:33	1	794	65.30	-22.97	104.73	15.43	131.11	1.0E+05	130.0
1977-01-18T20:15:46	2	150	82.38	-13.89	-2.30	6.46	188.38	4.0E+04	133.8
1977-01-19T22:44:45	2	151	82.55	-16.53	-29.25	6.44	189.02	3.9E+04	137.4
1977-01-27T16:09:27	2	158	84.03	-32.23	140.87	6.23	193.52	4.8E+04	143.4
1977-02-01T02:07:06	2	163	85.04	-39.68	31.40	6.05	196.12	3.9E+04	149.8

1977-02-03T07:06:31	2	165	85.60	-43.15	-23.79	5.94	197.42	5.0E+04	142.3
1977-02-04T09:35:21	2	166	85.87	-44.77	-51.24	5.88	198.07	4.0E+04	139.7
1977-02-12T03:02:16	2	172	88.01	-55.13	113.16	5.31	202.68	3.1E+04	145.8
1977-02-14T08:01:26	2	174	88.67	-57.70	56.40	5.09	204.00	3.2E+04	170.6
1977-02-17T15:31:33	2	176	89.70	-61.25	-30.14	4.69	206.00	3.1E+04	157.8
1977-02-26T11:28:33	2	185	92.57	-67.83	92.90	3.14	211.36	2.3E+04	180.3
1977-02-27T13:57:56	2	186	92.94	-68.29	62.59	2.90	212.03	2.2E+04	177.6
1977-04-08T19:34:50	2	225 ^w	85.41	64.04	157.22	12.73	237.09	4.3E+04	161.6
1977-04-10T20:31:57	2	227 ^w	85.81	64.03	164.07	12.81	238.38	5.9E+04	147.2
1977-04-12T21:28:38	2	229 ^w	86.24	64.04	171.07	12.90	239.66	3.7E+04	158.2
1977-11-25T14:49:39	2	464	82.39	54.99	-148.51	6.47	10.06	5.6E+04	122.2
1977-11-26T14:49:11	2	465	83.87	57.26	-141.65	6.29	10.54	5.9E+04	129.0
1977-12-02T14:50:05	2	471	90.55	66.87	-103.87	5.00	13.43	3.2E+04	142.5
1977-12-22T14:43:45	2	491	93.87	73.17	51.16	2.51	22.88	1.3E+04	159.9
1977-12-24T14:39:41	2	493	93.08	72.99	74.35	2.72	23.81	1.5E+04	155.6
1977-12-25T14:37:34	2	494	92.63	72.81	86.50	2.86	24.27	8.4E+03	166.2
1977-12-26T14:35:35	2	495	92.15	72.55	98.93	3.02	24.74	1.1E+04	156.3
1977-12-27T14:33:50	2	496	91.64	72.19	111.58	3.20	25.20	9.4E+03	152.0
1978-01-04T14:32:55	2	504	87.12	63.85	-148.04	4.78	28.90	4.1E+04	135.6
1978-01-06T14:35:58	2	506	86.08	59.84	-125.04	5.09	29.82	4.6E+04	137.5

1978-01-07T14:37:50	2	507	85.61	57.47	-113.91	5.23	30.28	4.6E+04	136.4
1978-01-08T14:39:51	2	508	85.19	54.89	-103.05	5.35	30.73	3.2E+04	131.1
1978-07-26T10:19:47	1	769 ^{s,x}	61.30	-13.10	-142.66	15.42	119.26	1.1E+05	120.6
1977-01-17T17:46:18	2	149 ^{p,x}	82.21	-11.03	24.76	6.48	187.75	5.1E+04	112.8
1977-01-17T17:46:18	2	149 ^{s,x}	82.21	-11.03	24.76	6.48	187.75	8.7E+04	142.3
1977-02-22T02:00:58	2	181 ^x	80.29	66.06	-61.51	10.23	208.68	8.6E+05	34.1

18 Figures

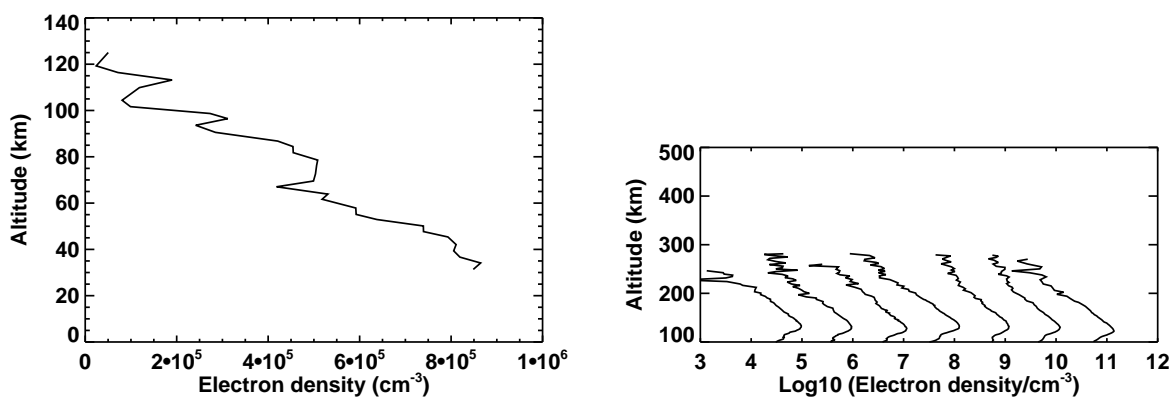


Figure 1: (left) Profile from Viking Orbiter 1 on orbit 181. (right) Profiles from Viking Orbiter 1 on orbits 610 (left), 612, 617, 622, 625, 626, and 639 (right). Densities in the i -th profile are multiplied by a factor of $10^{(i-1)}$ in order to offset profiles for clarity. That is, densities in the first profile (orbit 610) are multiplied by a factor of $10^0 = 1$ and densities in the seventh profile (orbit 639) are multiplied by a factor of 10^6 . Reproduction of Figure 9b of *Zhang et al.* (1990a).

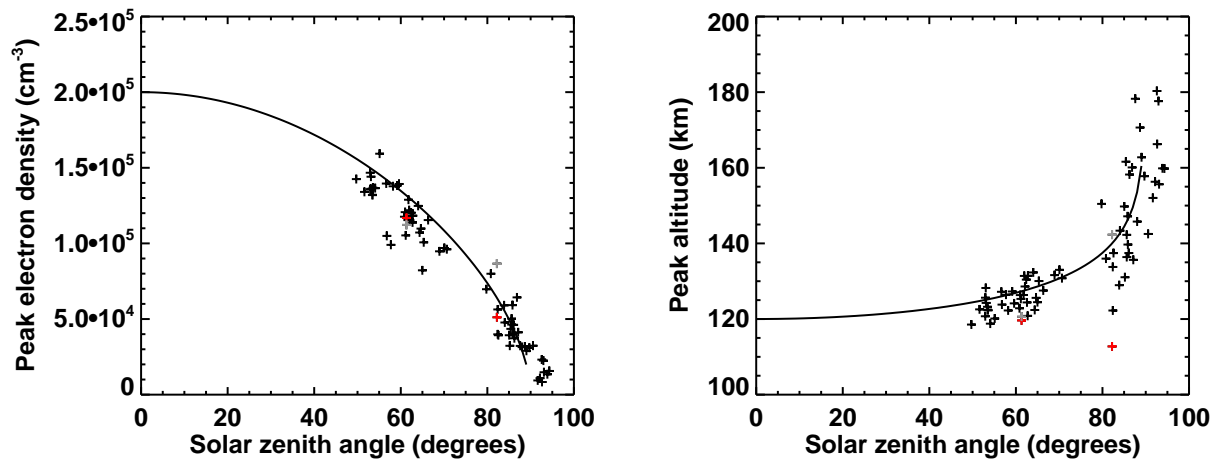


Figure 2: (left) Peak electron density as a function of solar zenith angle (crosses). The solid line is a fit from *Hantsch and Bauer* (1990). Reproduction of Figure 1 of *Hantsch and Bauer* (1990). (right) Peak altitude as a function of solar zenith angle (crosses). The solid line is a fit from *Hantsch and Bauer* (1990). Reproduction of Figure 3 of *Hantsch and Bauer* (1990).

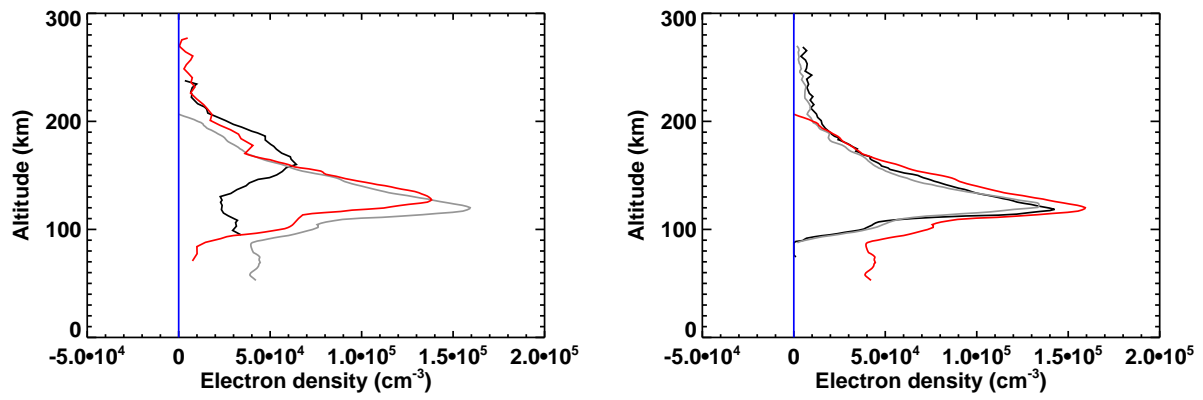


Figure 3: (left) Profiles from Viking Orbiter 1 on orbits 289 (black), 523 (grey), and 755 (red). The vertical blue line indicates zero. (right) Profiles from Viking Orbiter 1 on orbits 490 (black), 508 (grey), and 523 (red). The vertical blue line indicates zero.

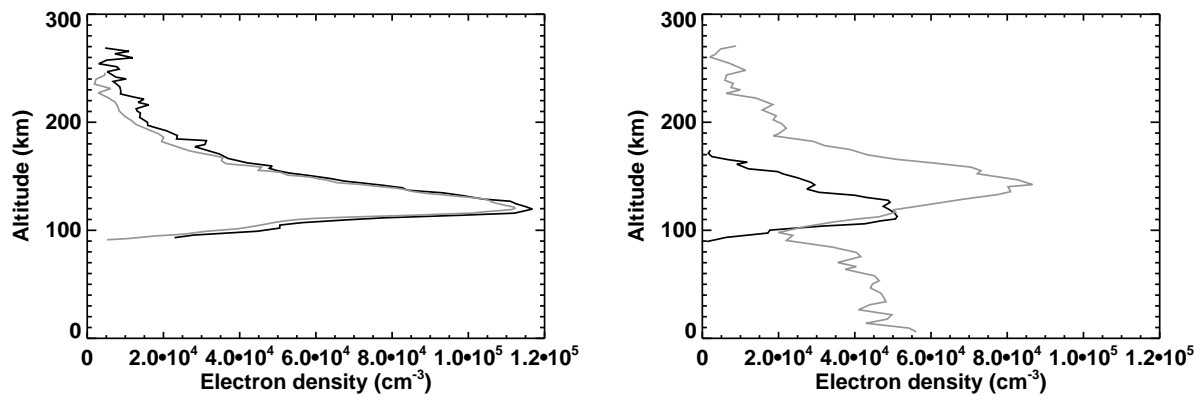


Figure 4: (left) Primary (black) and secondary (grey) representations of the profile from Viking Orbiter 1 on orbit 769. (right) Primary (black) and secondary (grey) representations of the profile from Viking Orbiter 2 on orbit 149.

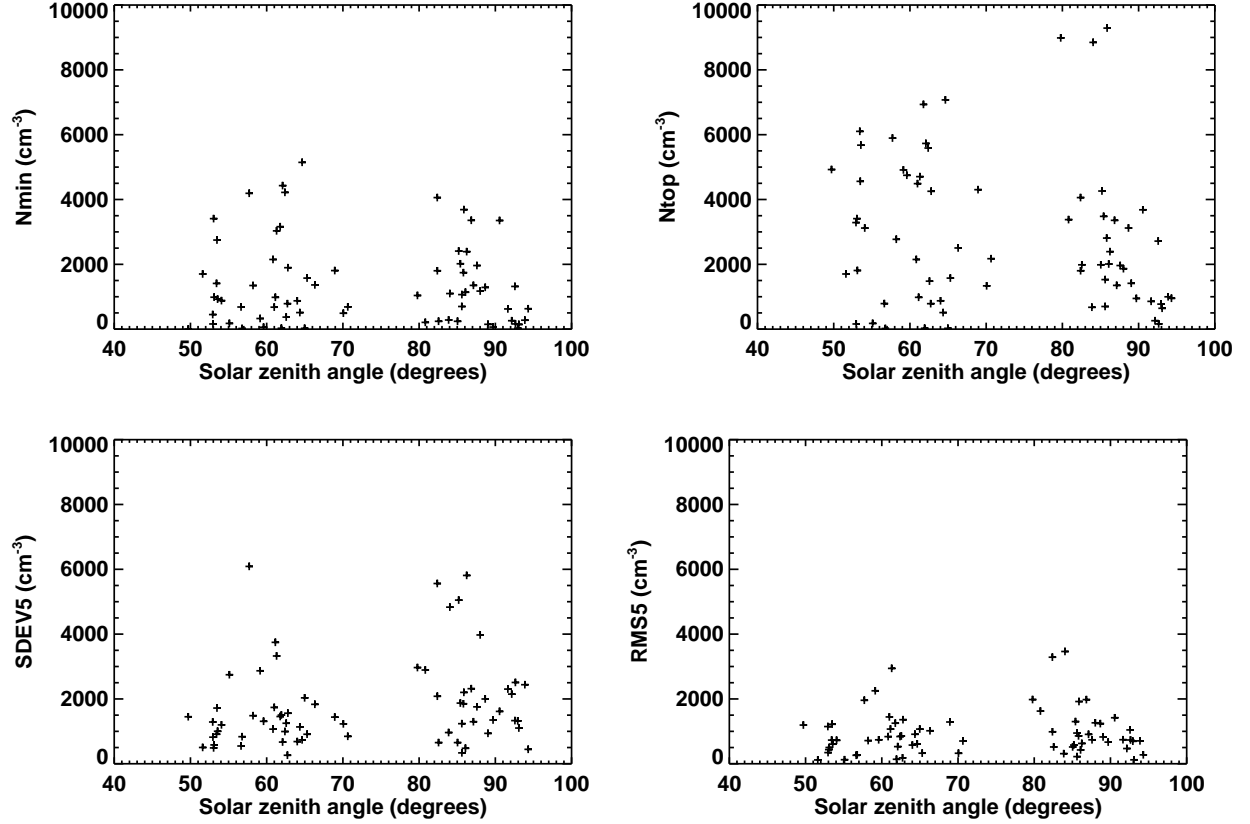


Figure 5: (top left) Dependence of N_{min} on solar zenith angle. (top right) Dependence of N_{top} on solar zenith angle. (bottom left) Dependence of $SDEV5$ on solar zenith angle. (bottom right) Dependence of $RMS5$ on solar zenith angle.

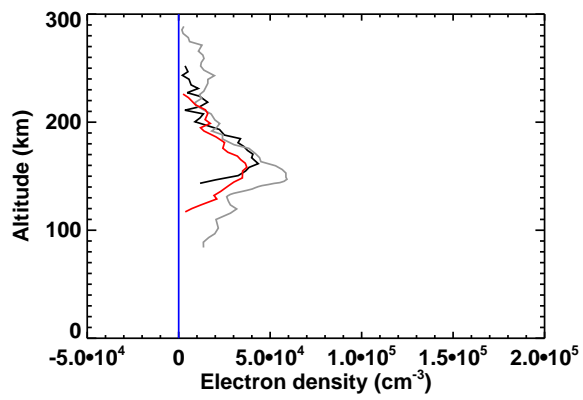


Figure 6: Profiles from Viking Orbiter 1 egress occultations on orbits 225 (black), 227 (grey), and 229 (red). The vertical blue line indicates zero.

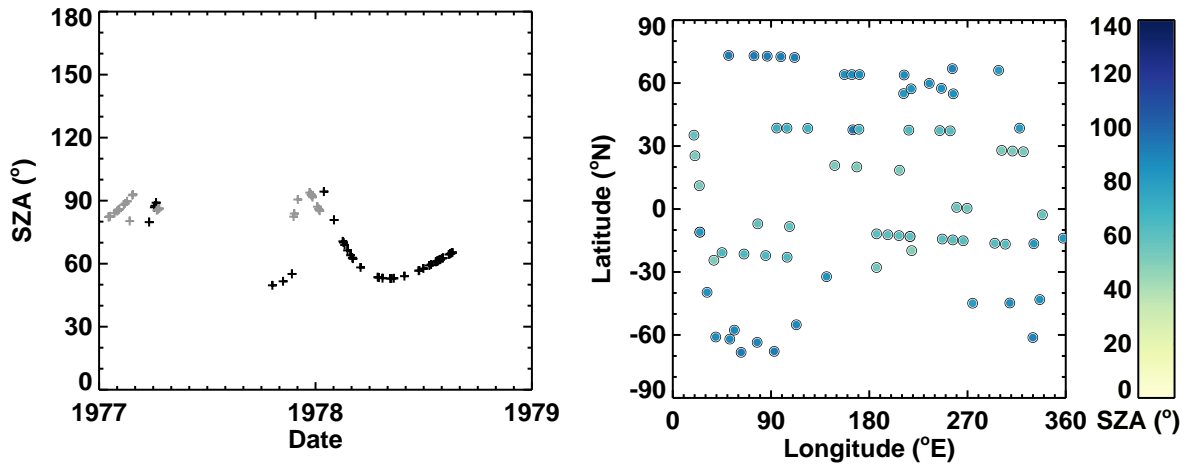


Figure 7: (left) Time series of solar zenith angles sampled by electron density profiles from Viking Orbiters 1 and 2 radio occultations. Black symbols indicate Viking Orbiter 1 profiles, grey symbols indicate Viking Orbiter 2 profiles. (right) Geographic coverage of electron density profiles from Viking Orbiters 1 and 2 radio occultations. Colors indicate solar zenith angle.

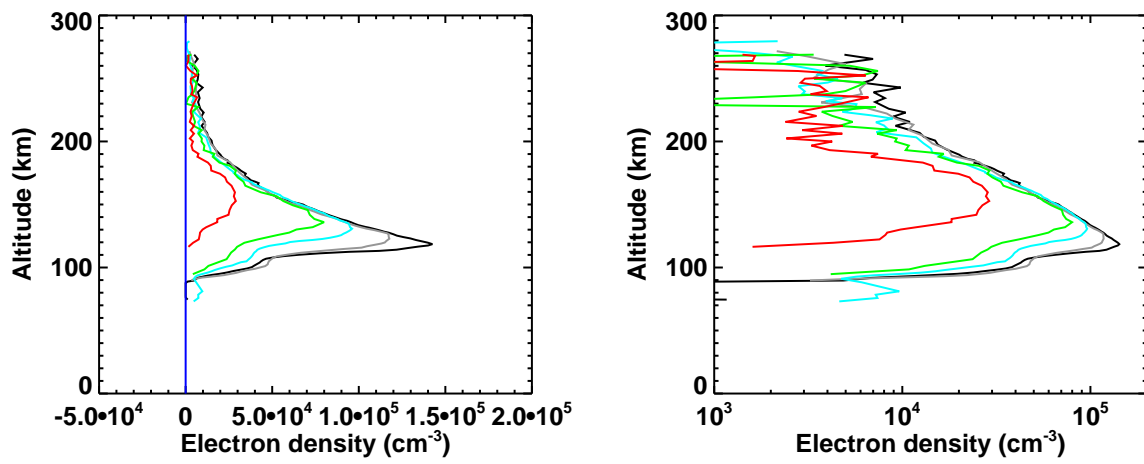


Figure 8: (left) Five selected profiles from Viking Orbiter 1 at solar zenith angles near 50° (orbit 490, black), 60° (orbit 766, grey), 70° (orbit 609, cyan), 80° (orbit 594, green), and 90° (orbit 292, red). The blue vertical line highlights zero. (right) As left panel, but with a logarithmic axis.

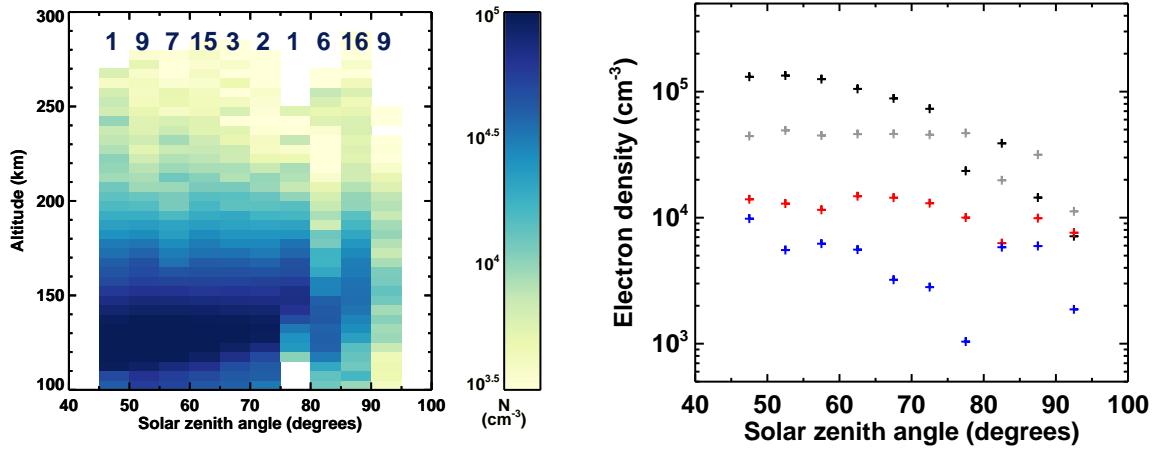


Figure 9: (left) Dependence of electron density on solar zenith angle and altitude. Regions without data are shown in white. The number of profiles in each solar zenith angle bin is noted at high altitude. (right) Electron density measurements from the left panel at altitudes of 120–125 km (black), 160–165 km (grey), 200–205 km (red), and 240–245 km (blue).